




Cite this: *Phys. Chem. Chem. Phys.*,
2022, **24**, 7732

Defects of thin CaO(001) on Mo(001): an EPR spectroscopic perspective†

Nina F. Richter and Thomas Risse *

Paramagnetic defects of thin CaO(001) films grown on Mo(001) are characterized using electron paramagnetic resonance (EPR) spectroscopy under ultrahigh vacuum conditions. A variety of paramagnetic centers located in the volume of the films are identified whose speciation as well as relative abundance was found to depend on the growth rate of the films. Pristine films prepared at a lower growth rate exhibited a larger number and a different speciation of paramagnetic defects than films grown at a higher rate. Annealing of the films to 1030 K, which improves their long-range order, results in quenching of most of the paramagnetic species observed for the pristine film; however, films prepared at a lower growth rate exhibit new paramagnetic signals upon annealing, which are absent in films prepared at a higher growth rate. The signals can be assigned to paramagnetic Mo ions previously shown to diffuse into these films. These results indicate that the amount and speciation of the transition metal ions depend on the preparation conditions which in turn can also affect the surface chemistry of these systems.

Received 24th January 2022,
Accepted 3rd March 2022

DOI: 10.1039/d2cp00389a

rsc.li/pccp

Introduction

Alkaline earth metal oxide materials such as CaO and MgO have various technological applications for instance in the fields of gas sensing and^{1,2} gas storage,³ and as a reactive surface or support system in heterogeneous catalysis.^{4–11} They have a rocksalt structure with comparable mechanical resistance,¹² thermal stability, optical properties,^{13,14} and band gap^{15,16} but they differ significantly in their chemical properties *e.g.* their basicity. As a result CaO interacts much stronger with adsorbates such as H₂O and CO₂ than the less basic MgO.^{17–19} In turn, atomic level characterization of CaO is significantly more challenging than that of MgO which is clearly mirrored by the number of studies being significantly larger for MgO. With respect to such a detailed characterization of oxide surfaces it has been shown that single crystalline oxide films grown epitaxially on metal supports are suitable model systems to gain microscopic insights for *e.g.* into the structural and electronic properties or the reaction behavior of the material.^{20–23} Among the alkaline earth oxides thin, epitaxial MgO films have been studied extensively,^{24–30} whereas investigations on CaO films are much more limited.^{31–35} The properties of alkaline earth oxide films being prototypical ionic oxides are known to be altered by defects such as dislocations, point defects or dopants.^{36–38}

Doping of the films with redox active aliovalent transition metal ions is another way to alter their electronic and chemical properties. This was exemplified for Mo doping of CaO(001)/Mo(001) films showing that Mo dopants enable a charge transfer from these centers to molecular adsorbates and metal particles altering their properties significantly.^{39–41} A detailed characterization of defects in general and transition metal ion impurities is however challenging. In this respect, EPR spectroscopy was shown to be a suitable technique in case paramagnetic impurities are present as demonstrated *e.g.* for Mo(v) centers present on the surface of MgO(001) films, which were also shown to participate in the redox processes on this surface.⁴²

In this study electron paramagnetic resonance (EPR) spectroscopy is used under ultrahigh vacuum (UHV) conditions to characterize paramagnetic defects of thin CaO(001) films grown on Mo(001). It is shown that the amount and speciation of paramagnetic defects depend on the growth conditions, *i.e.*, the deposition rate of Ca.

Experimental details

The experiments were performed in an ultra-high vacuum chamber with a base pressure of 2×10^{-10} mbar comprising a low-energy electron diffraction (LEED), a mass spectrometer (HAL, 201 Hiden), an EPR spectrometer (EMX, Bruker), an ion-gun (ISE 10, Omicron), and an EFM 3 evaporator (Omicron) which has been described in detail elsewhere.⁴³ Cleaning of the Mo(001) substrate was done by cycles of oxidation at 1500 K in

*Institut für Chemie und Biochemie, Freie Universität Berlin, Arnimallee 22,
14195 Berlin, Germany. E-mail: risse@chemie.fu-berlin.de*

† Electronic supplementary information (ESI) available. See DOI: 10.1039/d2cp00389a



O₂ (background pressure of 1×10^{-6} mbar) and subsequent annealing to 2300 K under UHV conditions. The preparation of CaO thin films follows a procedure described in detail elsewhere.³¹ In brief, the CaO film was prepared *via* a two-step procedure with each step involving evaporation of Ca from a molybdenum crucible in an oxygen ambient of 1×10^{-7} mbar (sample was biased to the voltage applied to the crucible). First, 5 ML of CaO was deposited at a rate of 2.4 \AA min^{-1} at room temperature and subsequently annealed to 1030 K. In a second step another 10 ML of CaO was deposited at room temperature with the rate stated in the text.

The CW-EPR measurements were obtained using a Bruker EMX spectrometer using a TE₁₀₂ resonator with a resonance frequency of about 9.5 GHz (X-Band), a microwave power of 2 mW, a modulation frequency of 100 kHz and a modulation amplitude of 3 Gauss. If not mentioned otherwise the spectra were recorded at 30 K which is the lowest temperature of the crystal attainable on cooling with liquid helium. The *g*-values were calculated referencing to a DPPH (2,2 diphenyl-1-picrylhydrazyl) standard ($g = 2.0036$) and the magnetic field axis was adjusted to account for the small difference in the microwave frequency between different measurements. The spectra presented here were carefully background corrected by subtracting the spectrum taken for the clean Mo(001) single crystal unless otherwise stated.

Results and discussion

Fig. 1a shows the EPR spectra of 15 ML CaO films taken after depositing 10 ML of CaO at room temperature onto a 5 ML CaO buffer layer (see the Experimental section for details) with Ca deposition rates of 2.4 \AA min^{-1} (Fig. 1a, black trace) and 3.6 \AA min^{-1} (Fig. 1a, green trace), respectively. The EPR spectra were recorded with the magnetic field oriented along the $\langle 110 \rangle$ direction of the Mo(001) surface. The black trace is dominated by an asymmetric line centered at $g = 2.0033$ with a peak-to-peak line width of 0.54 mT and a broad shoulder on the low-field side. In contrast to this, the spectrum of the film grown at a higher Ca desorption rate results in an EPR signal at $g = 2.0072$ with a peak-to-peak line width of ~ 1.6 mT (Fig. 1a, green trace). It is interesting to note that this signal matches the shoulder observed for the preparation at a lower deposition rate (black trace) suggesting that the formation of the corresponding paramagnetic species does not depend on the flux of Ca used (for the line shape of the subtracted spectra see Fig. S1, ESI[†]). A closer inspection of the signal observed for the higher Ca deposition rate (Fig. 1a, green trace) reveals the presence of a small narrow signal at $g = 2.0033$ which matches the position found for the low deposition rate (black trace), but with a significantly reduced intensity. The EPR spectra obtained after subsequent annealing of the CaO films to 1030 K under UHV conditions are shown in Fig. 1b keeping the color coding used above. The spectrum of the annealed CaO film grown with a low Ca/O₂ ratio (Fig. 1b, black trace) exhibits an almost symmetric line at $g = 2.0059$ with a line width of 0.6 mT and a reduced

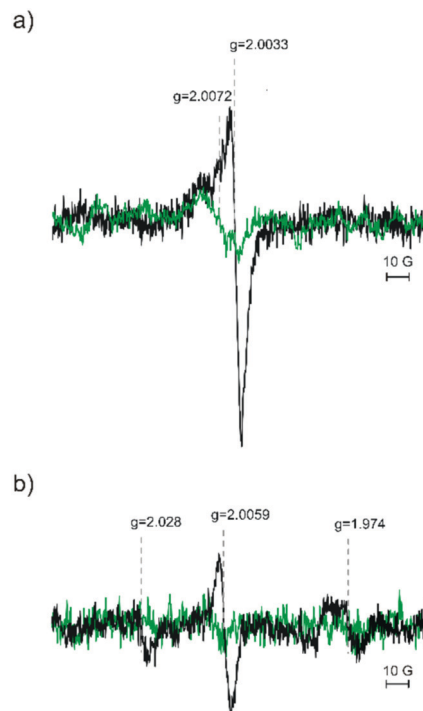


Fig. 1 EPR spectra of the 15 ML thick CaO(001) film grown on Mo(001). (a) 10 ML of CaO grown at RT on top of a 5 ML buffer layer with Ca deposition rates of 2.4 \AA min^{-1} ((a) black curve) and 3.6 \AA min^{-1} ((a) green trace), respectively. (b) The comparison of both CaO films upon annealing to 1030 K, Ca deposition rates of 2.4 \AA min^{-1} ((b) black curve) and 3.6 \AA min^{-1} ((b) green trace).

amplitude (about 50%) compared to the signal of the pristine film. Comparison of the signals generated under low Ca flux conditions (Fig. 1a and b, black trace) suggests that annealing results in the quenching of a signal located at $g = 2.0033$, which corroborated the other preparation methods in which the signal at $g = 2.0033$ is quenched after annealing (Fig. 1a and b, green traces). The EPR spectrum of the annealed CaO film grown with higher Ca flux exhibits a small signal at $g = 2.0072$ which has a significantly reduced intensity compared to that of the pristine film (Fig. 1b, green trace). Please note that the line shape of the spectrum observed for the annealed films grown with a low Ca flux (black trace) is consistent with a signal at $g = 2.0072$ having the same intensity as the one observed for the higher Ca flux (green trace). The similarity of this signal to that of the pristine films and its behavior upon annealing further corroborate the interpretation that this signal belongs to a paramagnetic species which is not altered by the Ca deposition rate. In addition, the black trace reveals two new signals at $g = 2.028$ and at $g = 1.974$ which are not found for the film grown with higher Ca flux. Further annealing to 1100 K which was previously reported to result in a partial dewetting of the film³⁹ leads to a quenching of the signal at $g = 2.028$ while the signal at $g = 1.974$ remained basically unaffected (Fig. S2, ESI[†]), which shows that these signals belong to two different paramagnetic species. As EPR spectroscopy is not inherently surface sensitive, 20 L of oxygen was adsorbed at 30 K on 15 ML thick



CaO as multilayers of oxygen were previously shown to quench the signal of paramagnetic species at the surface of oxides.³⁶ No significant signal quenching was observed (data not shown). Therefore, it is concluded that the paramagnetic species are located in the bulk of the CaO film.

While the shape of the signals around $g = 2$ differs significantly for the spectra shown in Fig. 1, three signals located at $g = 2.0033$, 2.0059 and 2.0072 can be clearly identified. Except for the spectrum observed for the pristine film grown under low Ca flux conditions (Fig. 1a, black trace) all other spectra may contain one or two of these components. As shown in Fig. 2 (red trace) the spectrum can be nicely fitted optimizing the relative intensity of the three components with fixed positions and line width as determined from other spectra: Fig. 1a, green trace: components at $g = 2.0072$ and $g = 2.0033$; Fig. 1b, black trace: component at 2.0059 . All four spectra can be fitted with these three spectral components and the resulting relative weights of the different components obtained from the fits are summarized in Table 1. Hence, the EPR spectra allow the discrimination of three paramagnetic species contributing to the signal pattern around the free electron g -value. The signal at $g = 2.0072$ is the one dominating the intensity of the EPR spectra of the pristine films irrespective of the Ca flux used. The two other components are less abundant. In case of low Ca flux preparation, these components amount to about 1/3 of the integral EPR intensity while the other preparation lacks the signal at $g = 2.0059$ and the signal at $g = 2.0033$ contributes only a few percent to signal intensity. The signal at $g = 2.0059$ is found only in the case of films grown under low Ca flux conditions and its intensity only slightly decreases upon annealing in contrast to the other two signals which are largely quenched upon annealing to 1030 K.

The quenching of an EPR signal around $g = 2$ upon annealing to about 1000 K was previously observed for MgO(001)/Mo(001) films grown at room temperature.⁴⁴ The EPR signal could be assigned to trapped electrons located at the grain

Table 1 Relative intensity of the different spectral components as revealed by fitting the four spectra shown in Fig. 1 with the spectral components shown in Fig. 2

Resonance Position (g)	2.0072	2.0059	2.0033
2.4 Å min ⁻¹ pristine	1 (70%)	0.13 (9%)	0.29 (21%)
2.4 Å min ⁻¹ annealed	Cannot be determined	1	0
3.6 Å min ⁻¹ pristine	1 (96%)	0	0.04 (4%)
3.6 Å min ⁻¹ annealed	1	0	0

boundaries of the MgO film.³⁸ Annealing of the MgO films improves their long range order, but these film still feature line defects. The latter exhibit trapping sites for electrons which can be filled *e.g.* by electron bombardment or reaction with hydrogen atoms.³⁷ Shao *et al.* showed that CaO films grown on top of a 5 ML buffer layer exhibit a Stranski–Krastanov type growth mode with good crystallinity already for growth at room temperature and coalescing islands for 10 ML thick films.³¹ The same study also showed that annealing of these films results in improving the long-range order of the film characterized by flat surface areas separated by line defects such as grain boundaries which run along $\langle 100 \rangle$ equivalent directions of the CaO film.

Hence, it is expected that exposure of the annealed CaO films to electrons will result in paramagnetic centers trapped electrons. Fig. 3 shows the EPR spectrum obtained after electron exposure (energy: 100 eV, dosage: 100 e⁻/surface O atoms; Fig. 3: black trace). The spectrum reveals a single line at $g = 2.0047$ with a line width of 0.5 mT which is slightly shifted compared to that of the pristine film ($g = 2.0033$). The characteristics of this line (position, line width, and intensity) depend somewhat on the preparation conditions indicating some distribution of the local environment of the trapping sites which cannot be resolved at the X-band. The intensity of the signal is significantly larger than that observed for all the pristine films. The EPR signal cannot be altered by exposure to 50 L of molecular oxygen at 30 K (Fig. 3, green trace) showing that

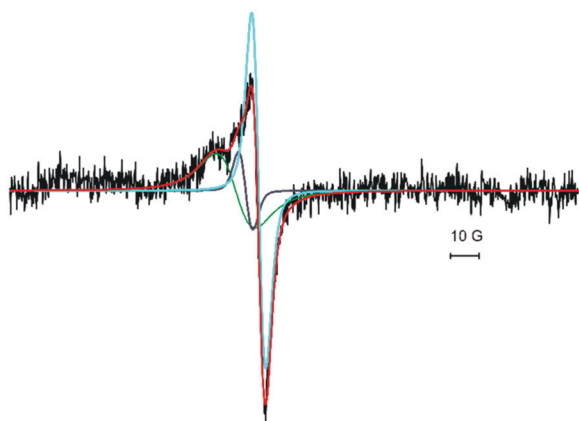


Fig. 2 The EPR spectrum of a 15 ML thick CaO film grown at room temperature at a Ca deposition rate of 2.4 Å min⁻¹ (black trace, see Fig. 1a) and the fit to the spectrum (red trace) being the sum of three components positioned at $g = 2.0033$, 2.0059 and 2.0072 . The individual components of the fit are shown in light blue, dark grey and green, respectively.

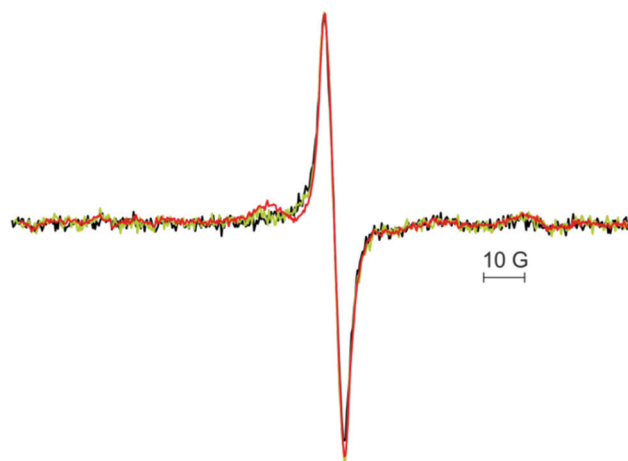


Fig. 3 The EPR spectra of a 15 ML thick annealed CaO film on Mo(001) after bombardment with electrons (100 eV) (black trace), subsequent adsorption of 50 L of oxygen at 30 K (green trace) and annealing to 300 K (red trace).



the paramagnetic species are located in the bulk of the CaO film in line with the expectations. Desorption of physisorbed oxygen by annealing to 300 K (Fig. 3, red trace) retains the signal at $g = 2.0047$ and results in an additional small signal on its low-field side. The latter disappears after annealing to 500 K, which also results in a reduction of the signal at $g = 2.0047$. Fig. 4 shows the EPR spectra after stepwise annealing of the film to 1030 K (for integral intensity see the inset). The intensity of the line at $g = 2.0047$ is reduced upon annealing and the signal disappears after annealing to 900 K. The latter spectrum shows a signal at $g = 2.0078$ which is already discernable for the film annealed at 700 K. Its intensity is reduced upon annealing to 1030 K. This signal is very similar to the one observed for the pristine films ($g = 2.0072$) indicating a close similarity of the species. More importantly it suggests that temperature induced quenching of the paramagnetic species does not alter in the local environment drastically as electron bombardment can reestablish the EPR signal.

Based on these observations and previous results found for MgO(001)/Mo(001)-films the signal at $g = 2.0033$ as well as the one found at $g = 2.0045$ after annealing and subsequent electron bombardment can be assigned to trapped electrons that are located in the grain boundaries of the CaO film. The small change of the g -value found for the annealed film can be related to the structural changes of the film upon annealing also altering the atomic structure of the grain boundaries. This is also in-line with previous reports on F^+ -centers and trapped electrons centers in CaO characterized by EPR signals around the free electron g -value.^{45–47} Apart from F^+ -centers and trapped electrons also oxygen centered radical species (hole centers) were characterized using EPR spectroscopy.^{48–52} While F^+ -centers and trapped electrons are characterized by an almost isotropic g -tensor, the oxygen centered radicals exhibit a

significant g -tensor anisotropy. Hole centers such as a classical O^- -center were reported to have an axial g -tensor with g_{par} around the free electron values and g_{perp} in the range of 2.07.⁴⁶ Due to the fourfold in-plane symmetry of the CaO film, the lack of signals with g -values larger than 2.0072 renders the observed spectra incompatible with well-defined oxygen centered radicals in the pristine films. However, it is important to keep in mind that the value of g_{perp} is rather sensitive to the environment and can vary significantly for different local environments. In turn, signals corresponding to B oriented along g_{perp} will be strongly broadened in the case of site heterogeneity.^{49,53} For small signal intensities present in such thin film samples, such broadening renders such a signal undetectable. In this respect, the line width of the signal at $g = 2.0072$ being considerably broader than that of the other signals around $g = 2$ would allow such an interpretation. Irrespective of the precise nature of the site the observed g -value does not match that of the reported species in CaO samples. A possible explanation is the location of these species at the interface between the buffer layer and the 10 ML CaO film as the buffer layer was found to be an ordered mixed oxide with Ca_3MoO_4 stoichiometry formed to accommodate the lattice strain.⁵⁴ In the vicinity of the interface the properties of paramagnetic species may thus be considerably altered as compared to those of stoichiometric CaO.

With respect to the signal at $g = 2.0072$ the results presented above showed that the formation of these centers does not depend on the growth rate and more importantly the quenching of the signal upon annealing can be reversed by electron bombardment which suggests that upon quenching of the signal the structural environment hosting the paramagnetic center is not altered strongly. Such a behavior is expected for trapped species such as hole centers or a thermally induced redox process. With respect to redox processes, previous STM and photoemission experiments showed that CaO films grown on Mo(001) are doped by Mo ions which can adopt various oxidation states depending on the preparation conditions.³² The diffusion of Mo ions into the CaO films leads to a downshift of the conduction band onset with increasing annealing temperature, an effect that decreases with increasing film thickness.^{32,39} A more detailed analysis of XPS data showed the presence of Mo species in the oxidation states between IV and VI . In particular, annealing above 900 K results in the formation of Mo species in the higher oxidation states (V and VI) preferentially located close to the surface of CaO films.³² This is consistent with theory predicting a temperature dependent stability of different oxidation states of Mo dopants in CaO.⁴¹ Mo-doping of CaO films was shown to alter the surface chemistry of the system. In particular, redox-active Mo ions can transfer electrons to molecules or deposited metal particles resulting for *e.g.* in negatively charged oxygen molecules.⁴⁰ Please note that the effect of doping metal oxides with aliovalent transition metal ions on the surface chemistry and the electronic structure of these materials is not limited to the thin film system, but also apply to powdered materials oftentimes exhibiting sizable amounts of transition metal impurities.

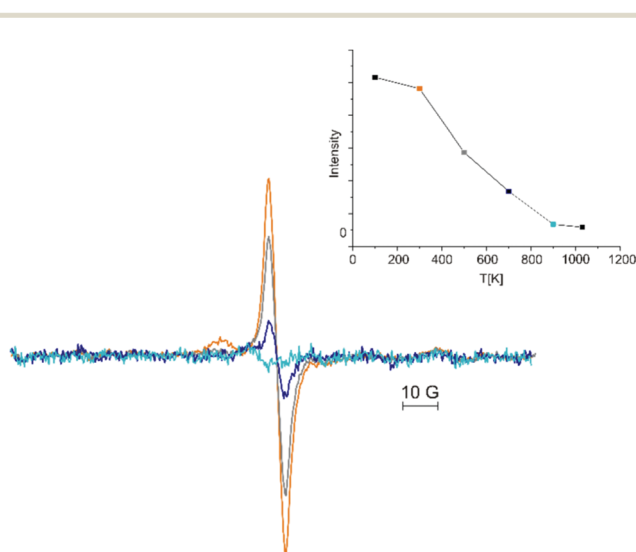


Fig. 4 The EPR spectra demonstrate a 15 ML CaO film at first bombarded with electrons, subsequent adsorption of 50 ML of oxygen and followed by successive annealing from 300 K to 1030 K. CaO films annealed to 300 K (red trace), to 500 K (grey trace), to 700 K (dark blue trace) and to 900 K (light blue trace).



Table 2 Observed paramagnetic signals and their assignments

Resonance position (g)	Conditions	Assignment
2.0033	Pristine films	Trapped electron
2.0045	After electron bombardment of annealed films	Trapped electron
2.0059	A film prepared at lower growth rate	—
2.0072	Independent of growth rate	Oxygen centered species at the interface to the buffer layer
1.97	A low growth rate; after annealing to 1030 K	Mo(v) center
2.028	A low growth rate; after annealing to 1030 K	Mo(III) center (tentatively)

Among the different paramagnetic states of Mo-ions, EPR signals of Mo(v) centers were reported for several Mo-doped oxides characterized by g -values below $g = 2$.^{55–57} In particular, such centers were found after annealing of MgO(001)-films on Mo(001) by EPR spectroscopy exhibiting g -values around 1.927.⁴² While these results do not allow for an assignment of signals with $g > 2$, they allow assigning the signal at $g = 1.974$ observed after annealing of the film prepared under low Ca flux conditions. Based on the results for Mo-doped MgO-films and the formation of Mo(v, vi) species upon annealing above 900 K mentioned above, the observed signal at $g = 1.974$ can be assigned to Mo(v) species.

With respect to the signal at $g = 2.028$ an assignment is less straightforward. The resonance position could be in line with oxygen based radical centers in a well-defined geometric environment exhibiting a suitable orientation of the corresponding g -tensor with respect to the lattice. However, the thermal stability of such species in CaO was reported to be low.⁵⁰ The XPS investigation provides evidence for the presence of other paramagnetic oxidation states of molybdenum. While EPR spectra d^2 and d^4 ions have not been reported in oxide materials, Mo(III)-ions are possible paramagnetic centers, too. These ions are isoelectronic to Cr(III) which is a d^3 -ion showing a signal around $g = 1.97$ if substituted into octahedral sites of CaO.⁴⁶ The simple EPR spectrum of the Cr(III) ions is enforced by the octahedral symmetry of lattice sites. In the case of distorted sites as for *e.g.* expected in grain boundaries, the EPR spectra will become much more complex, because the zero-field splitting will no longer be enforced to be 0.⁵⁸ A sizable zero-field splitting has a significant impact on the resonance position. Given the structural rearrangements observed during annealing and the presence of Mo(III) species inferred from the XPS results, a tentative assignment of the signal at $g = 2.028$ to Mo(III) ions is plausible. It is important to note that the presence of the Mo-related EPR signal depends on the growth conditions of the CaO film (Fig. 1b). A dependence of Mo diffusion into the oxide film was also reported for MgO-films.⁴² Mo-doping of CaO(001)/Mo(001)-films is known to reduce the lattice strain in this system,³¹ which provides an energetic driving force for Mo-doping. However, the level of Mo-doping will depend on the kinetics of the corresponding diffusion process and hence, a dependence on the preparation conditions is conceivable. Different levels of Mo doping in the pristine films influence the residual strain in the lattice, which can impact the stability of defect sites and allows the understanding of the dependence of the paramagnetic species characterized by the signal at $g = 2.0059$ on the growth rate (Table 2).

Conclusions

Using EPR spectroscopy under UHV conditions it was possible to identify three different paramagnetic defects for pristine 15 ML thick CaO films grown on Mo(001) at room temperature whose relative amounts depend on the Ca deposition rate. The three paramagnetic species for the pristine film were all located in the bulk of the film. The one at the lowest g -value ($g = 2.0033$) is readily assigned to trapped electrons at grain boundaries. This is further corroborated by electron bombardment of the annealed film, which results in a very intense signal at a slightly higher g -value which is consistent with the expectations based on structurally modified grain boundaries for the annealed film. While the intensity of the signal at $g = 2.0033$ differs significantly for the two growth rates, the behavior of the signal at $g = 2.0072$ is independent of the preparation conditions. In particular, annealing to 1030 K reduces its intensity significantly, but subsequent electron bombardment reestablished the species as inferred from the g -value of the signal and its thermal stability. The third signal at $g = 2.0059$ observed for the pristine films was exclusively found for films grown under low Ca flux conditions. These films also show two new signals after annealing to 1030 K whereas the EPR spectra of annealed films grown at a higher Ca rate lack new signals. The signal at $g = 1.974$ can be assigned to Mo(v) species indicating that the amount and speciation of Mo-species in the CaO films depend on the growth rate of the film, which also implies that the surface chemistry of the films previously shown to be altered by redox active Mo dopants will depend on such parameters.

Author contributions

The manuscript was written through contributions from both authors. Both authors have given approval to the final version of the manuscript.

Conflicts of interest

The authors declare no competing financial interest.

Acknowledgements

We acknowledge financial support from the German Research Foundation (DFG) through SFB1109. N. F. R. thanks the International Max-Planck Research School “Functional Interfaces in Physics and Chemistry” for support.



References

- 1 F. Bebensee, F. Voigt and W. Maus-Friedrichs, *Surf. Sci.*, 2008, **602**, 1622–1630.
- 2 K. T. Philemon and K. K. Korir, *J. Phys.: Condens. Matter*, 2020, **32**, 245901–245906.
- 3 S. Tian, J. Jiang, D. Hosseini, A. M. Kierzkowska, Q. Imtiaz, M. Broda and C. R. Müller, *ChemSusChem*, 2015, **8**, 3839–3846.
- 4 A. Tsiotsias, N. D. Charisiou, I. V. Yentekakis and M. A. Goula, *Catalysts*, 2020, **10**, 2073–4344.
- 5 D. Méndez-Mateos, V. L. Barrio, J. M. Requies and J. F. Cambra, *Catalysts*, 2021, **11**, 353–379.
- 6 C. Liang, X. Hua, T. Wei, P. Jia, Z. Zhang, D. Donga, S. Zhang, Q. Liuc and G. Hu, *Int. J. Hydrogen Energy*, 2019, **44**, 8197–8213.
- 7 V. R. Choudhary, M. R. Aniarjeet and B. Prabhakar, *Angew. Chem., Int. Ed. Engl.*, 1994, **33**, 2104.
- 8 X. D. Peng and P. C. Stair, *J. Catal.*, 1991, **128**, 264–274.
- 9 T. Grzybek, G. C. Maiti, D. Scholz and M. Baerns, *Appl. Catal.*, 1993, **107**, 115–124.
- 10 D. M. Reinoso, S. Angeletti, P. M. Cervellini and D. E. Boldrini, *Braz. J. Chem. Eng.*, 2020, **37**, 679–690.
- 11 M. A. Rezvani and N. Jafari, *Ind. Eng. Chem. Res.*, 2021, **60**, 7599–7610.
- 12 A. J. Cinthia, G. S. Priyanga, R. Rajeswarapalanichamy and K. Iyakutti, *J. Phys. Chem. Solids*, 2015, **79**, 23–42.
- 13 P. Myrach, N. Nilius, S. V. Levchenko, A. Gonchar, T. Risse, K. Dinse, L. A. Boatner, W. Frandsen, R. Horn, H.-J. Freund, R. Schlögl and M. Scheffler, *ChemCatChem*, 2010, **2**, 854–862.
- 14 S. K. Medeiros, E. L. Albuquerque, F. F. Maia, E. W. S. Caetano, G. A. Farias, V. N. Freire, B. S. Cavada, M. L. Pessati and T. L. P. Pessati, *Microelectron. J.*, 2005, **36**, 1058–1061.
- 15 R. C. Whited, C. J. Flaten and W. C. Walker, *Solid State Commun.*, 1973, **11**, 1903–1905.
- 16 G. Cappellini, S. Bouette-Russo, B. Amadon, C. Noguera and F. Finocchi, *J. Phys.: Condens. Matter*, 2000, **12**, 3671–3688.
- 17 M. J. D. Low, N. Takezawa and A. J. Goodsel, *J. Colloid Interface Sci.*, 1971, **37**, 422–429.
- 18 Y. Fukuda and K. Tanabe, *Bull. Chem. Soc. Jpn.*, 1973, **46**, 1616–1619.
- 19 P. Liu, T. Kendelewicz, G. E. Brown Jr., G. A. Parks and P. Pianetta, *Surf. Sci.*, 1998, **416**, 326–340.
- 20 H. J. Freund, H. Kuhlenbeck and V. Staemmler, *Rep. Prog. Phys.*, 1996, **59**, 283–347.
- 21 C. Xu and D. W. Goodman, in *Handbook of Heterogeneous Catalysis*, ed. G. Ertl, H. Knözinger and J. Weitkamp, Wiley-VCH, Weinheim, 1997, vol. 2, p. 826.
- 22 *Oxide Materials at the Two-Dimensional Limit*, ed. F. P. Netzer and A. Fortunelli, Springer, Heidelberg, 2016.
- 23 H.-J. Freund, M. Heyde, H. Kuhlenbeck, N. Nilius, T. Risse, S. Schaueremann, T. Schmidt, S. K. Shaikhutdinov and M. Sterrer, in *Handbook of Surface Science*, ed. M. Rocca, T. S. Rahman and L. Vattuone, Springer, 2021, p. 267.
- 24 M. C. Wu, J. S. Corneille, C. A. Estrada, J. W. He and D. W. Goodman, *Chem. Phys. Lett.*, 1991, **182**, 472–478.
- 25 M. C. Wu, C. M. Truong, K. Coulter and D. W. Goodman, *J. Am. Chem. Soc.*, 1992, **114**, 7565–7567.
- 26 M. C. Gallagher, M. S. Fyfield, L. A. Bumm, J. P. Cowin and S. A. Joyce, *Thin Solid Films*, 2003, **445**, 90–95.
- 27 J. Wollschläger, D. Erdos, H. Goldbach, R. Hopken and K. M. Schröder, *Thin Solid Films*, 2001, **400**, 1–8.
- 28 S. Schintke, S. Messerli, M. Pivetta, F. Patthey, L. Libioulle, M. Stengel, A. De Vita and W.-D. Schneider, *Phys. Rev. Lett.*, 2001, **87**, 2768011–2768014.
- 29 M. Kiguchi, T. Goto, K. Saiki, T. Sasaki, Y. Iwasawa and A. Koma, *Surf. Sci.*, 2002, **512**, 97–106.
- 30 S. Benedetti, H. M. Benia, N. Nilius, S. Valeria and H. J. Freund, *Chem. Phys. Lett.*, 2006, **430**, 330–335.
- 31 X. Shao, P. Myrach, N. Nilius and H.-J. Freund, *J. Phys. Chem. C*, 2011, **115**, 8784–8789.
- 32 Y. Cui, Y. Pan, L. Pascua, H. Qiu, C. Stiehler, H. Kuhlenbeck, N. Nilius and H.-J. Freund, *Phys. Rev. B: Condens. Matter Mater. Phys.*, 2015, **91**, 035418.
- 33 Y. Fujimori, X. Zhao, X. Shao, S. V. Levchenko, N. Nilius, M. Sterrer and H.-J. Freund, *J. Phys. Chem. C*, 2016, **120**, 5565–5576.
- 34 B. H. Solis, Y. Cui, X. F. Weng, J. Seifert, S. Schaueremann, J. Sauer, S. Shaikhutdinov and H. J. Freund, *Phys. Chem. Chem. Phys.*, 2017, **19**, 4231–4242.
- 35 J. Seifert, S. J. Carey, S. Schaueremann, S. Shaikhutdinov and H. J. Freund, *Top. Catal.*, 2021, **64**, 1030–1040.
- 36 M. Sterrer, E. Fischbach, T. Risse and H.-J. Freund, *Phys. Rev. Lett.*, 2005, **94**, 1079–7114.
- 37 H.-M. Benia, P. Myrach, A. Gonchar, T. Risse, N. Nilius and H.-J. Freund, *Phys. Rev. B: Condens. Matter Mater. Phys.*, 2010, **81**, 2414151–2414154.
- 38 D. Cornu, J. Rucker, A. Gonchar, T. Risse and H.-J. Freund, *Phys. Rev. Lett.*, 2016, **117**, 0168011–0168015.
- 39 X. Shao, S. Prada, L. Giordano, G. Pacchioni, N. Nilius and H.-J. Freund, *Angew. Chem., Int. Ed.*, 2011, **50**, 11525–11527.
- 40 Y. Cui, X. Shao, M. Baldofski, J. Sauer, N. Nilius and H.-J. Freund, *Angew. Chem., Int. Ed.*, 2013, **52**, 11385–11387.
- 41 S. Prada, L. Giordano and G. Pacchioni, *J. Phys. Chem. C*, 2013, **117**, 9943–9951.
- 42 A. Gonchar and T. Risse, *Mol. Phys.*, 2013, **111**, 2708–2716.
- 43 J. Schmidt, T. Risse, H. Hamann and H.-J. Freund, *J. Chem. Phys.*, 2002, **116**, 10861–10868.
- 44 A. Gonchar, PhD thesis, Freie Universität Berlin, 2011.
- 45 J. E. Wertz, J. W. Orton and P. Auzins, *Discuss. Faraday Soc.*, 1961, **31**, 140–150.
- 46 B. Henderson and J. E. Wertz, *Adv. Phys.*, 1968, **17**, 749–855.
- 47 M. Chiesa, M. C. Paganini, E. Giamello, C. Di Valentin and G. Pacchioni, *ChemPhysChem*, 2006, **7**, 728–734.
- 48 M. M. Abraham, Y. Chen, L. A. Boatner and R. W. Reynolds, *Solid State Commun.*, 1975, **16**, 1209–1213.
- 49 W. P. Unruh, Y. Chen and M. M. Abraham, *J. Chem. Phys.*, 1973, **59**, 3284–3288.
- 50 D. Cordischi, V. Indovina and M. Occhiuzzi, *J. Chem. Soc., Faraday Trans. 1*, 1978, **74**, 883–892.
- 51 M. C. Paganini, M. Chiesa, F. Dolci, P. Martino and E. Giamello, *J. Phys. Chem. B*, 2006, **110**, 11918–11923.



- 52 M. C. Paganini, M. Chiesa, P. Martino, E. Giamello and E. Garrone, *J. Phys. Chem. B*, 2003, **107**, 2575–2580.
- 53 M. M. Abraham, W. P. Unruh and Y. Chen, *Phys. Rev. B: Solid State*, 1974, **10**, 3540.
- 54 X. Shao, P. Myrach, H.-J. Freund, U. Martinez, S. Prada, L. Giordano and G. Pacchioni, *Phys. Rev. B: Condens. Matter Mater. Phys.*, 2011, **83**, 245407.
- 55 K. N. Spiridonov, G. B. Pariiskii and O. V. Krylov, *Bull. Acad. Sci. USSR*, 1970, 2646–2647.
- 56 D. Nikolova, R. Edreva-Kardjieva, G. Gouliev, T. Grozeva and P. Tzvetkov, *Appl. Catal., A*, 2006, **297**, 135–144.
- 57 R. Stösser, U. Marx, W. Herrmann, J. K. Jabor and A. Brückner, *J. Am. Chem. Soc.*, 2010, **132**, 9873–9880.
- 58 W. D. Ohlsen, *Phys. Rev. B: Solid State*, 1973, **7**, 4058–4060.

